

Nucleation and Growth Mechanism of Electro-synthesized Poly(pyrrole) on Steel

G. C. Arteaga¹, M. A. del Valle^{1,*}, M. Antilén¹, M. Romero¹, A. Ramos¹, L. Hernández¹,
M. C. Arévalo², E. Pastor², G. Louarn³

¹ Pontificia Universidad Católica de Chile, Facultad de Química, Departamento de Química Inorgánica, Laboratorio de Electroquímica de Polímeros (LEP), Vicuña Mackenna 4860, 7820436, Macul, Santiago, Chile.

² Universidad de La Laguna, Facultad de Química, Departamento de Química Física, 38071-La Laguna, Tenerife, España.

³ Université de Nantes, Institut Jean Materieux Rousel (IMN), CNRS, UMR 6205, 2 rue de la Houssinière, BP 32229, 44322, Nantes Cedex 3, France.

*E-mail: mdvalle@uc.cl

Received: 7 January 2013 / Accepted: 29 January 2013 / Published: 1 March 2013

Polypyrrole was electro-synthesized by potentiodynamic and potentiostatic methods on AISI 316 stainless steel (SS) using lithium perchlorate as supporting electrolyte and acetonitrile as solvent to obtain the respective polymeric coating. One of the most relevant characteristics of this polymer is that its voltammetric response showed the presence of reversible p- and n-doping/undoping processes. Moreover, nucleation and growth mechanisms (NGM) were established by i/t transients deconvolution recorded during the potentiostatic electro-polymerization. It was found that the overall process mechanism involved two contributions, namely an instantaneous nucleation with two-dimensional growth (IN2D) and a three-dimensional progressive nucleation with diffusion-controlled growth (PN3D_{diff}). The nuclei shape predicted by these NGMs are consistent with the respective morphologies obtained by SEM and AFM, which validates, once more, the proposed electro-polymerization model and the predictions from the NGM morphology of the respective electro-deposited polymer. In short, a correlation between the structure of the starting unit, doping and morphology of the electro-deposited polymer was established. At the same time conditions for the electro-obtention of this widely studied polymer were optimized, but this time on SS, a cheap electrodic substrate that makes its potential application more feasible.

Keywords: pyrrole, polypyrrole, nucleation and growth mechanism, n-doping, p-doping.

1. INTRODUCTION

Poly(pyrrole), Ppy, has been one of the most studied conducting polymers and used in different applications, the most relevant being fuel cells, materials for artificial muscles, as heavy metals

extractor, carbon nanotubes fabrication, counter electrode for solar cells coating. Besides, often used as a biosensor and gas sensor, anti-electrostatic coating, solid electrolytic capacitor, electrochromic windows, displays, polymer batteries, electronic devices, functional membranes, etc. [1-14].

In the last century, Ppy was one of polymers with more publications, mainly due to the aforementioned applications. The purpose of the current work was to accomplish and contribute to the understanding of Ppy nucleation and growth mechanism on SS, because derivatives from this monomer have been previously studied on this substrate [15] and have been analyzed and characterized. However, py has not been studied under these conditions, which is essential not only for the sake of comparison, but also because offers a cheap and affordable working medium and electrode.

Electro-synthesis will enable *in situ* characterization using potentiodynamic (cyclic voltammetry, CV) and potentiostatic techniques that will lead to establish, respectively, the *doping/undoping* processes and the nucleation and growth mechanism (NGM). The latter will be correlated with morphological results, to be performed by scanning electron microscopy (SEM) and atomic force microscopy (AFM), to verify if the NGM allows predicting morphology, as already established in other cases [16-25]. Besides, a correlation between morphology and starting unit structure and with their macroscopic properties, *e.g.* conductivity and type of *doping*, will be searched for.

2. EXPERIMENTAL

All aqueous solutions were prepared with freshly deionized water on a Heal Force (Smart Series) deionizer. All measurements were performed at room temperature (20 °C) under high purity argon atmosphere in three-compartment anchor-type electrochemical cells. The working electrode was a 0.07 cm² geometric area AISI 316 steel disc (SS). The counter electrode was a platinum wire coil of large geometric area. Ag/AgCl in tetramethylammonium chloride solution, its potential adjusted to that of a saturated calomel electrode, SCE, was utilized [39] as reference electrode. Unless otherwise stated, all potentials quoted in the current work are referred to this electrode at room temperature.

Py (Aldrich, 98%) electro-oxidation on SS was optimized in cell assemblies under the abovementioned conditions. The electro-polymerization was carried out using successive potentiodynamic scans (CV), potential scan rate 50 mV·s⁻¹ and within different potential windows. Solutions having different monomer concentrations and various supporting electrolytes were employed.

Thus, after numerous trials, optimal conditions that enabled working with the four proposed starting units were as follows. 0.01 mol·L⁻¹ monomer solution in 0.1 mol·L⁻¹ lithium perchlorate (LiClO₄ 99%, Aldrich) supporting electrolyte in 99.8% acetonitrile (CH₃CN, Aldrich) as solvent, the latter being suitable for working within the -0.6 and 1.5 V window.

From these results, the potentiostatic method (PM) was tried. The optimum potential to prepare the SS/Ppy electrode in this medium was 1.36 V. According to the specific goal, electrolysis time ranged between 1 and 30 min.

In each case, to optimize the conditions to be employed, the stable electrochemical response of the modified electrode in a solution containing just supporting electrolyte was determined. This enabled the respective *p-doping/undoping* and *n-doping/undoping* processes to be analyzed in order to find the amount of charge involved and, especially, the most reversible response.

All electrochemical measurements (polymerization and characterization) were performed on an Autolab PGSAT 20 potentiostat. Furthermore, to observe the morphology of each polymeric deposit, analyses were conducted using SEM on a JEOL, Model 6300F, Scanning Electron Microscope. Then, to detail the morphology and topography of the polymer, AFM measurements were made on a Digital Instruments Nanoscope Multi-Mode AFM-2 at the University of La Laguna, Spain. Finally, to complement the characterization Fourier Transform Infrared - Attenuated Total Reflectance (ATR) spectroscopy measurements were accomplished on an IFS 66/S BRUKER spectrometer, and Raman spectroscopy measurements were carried out on a Bruker RF S100 spectrometer (excitation wavelength 1064 nm).

3. RESULTS AND DISCUSSION

The voltammetric profile in Fig. 1 depicts py electrochemical oxidation after 50 successive CV cycles, under the experimental conditions (concentration, supporting electrolyte) and within the optimum working window set forth herein. Current increase between consecutive cycles is an evidence of polymer growth, along with the clear presence of *p-* (between 0.0 and 1.0 V) and *n-doping/undoping* (between 0.0 and -0.6 V) processes.

Besides of evidencing the *n-doping/undoping* processes, these profiles allow establishing the nucleation and growth region, around 1.5 V. The optimum working potential for the potentiostatic method should thus be searched for in this region, Fig. 2.

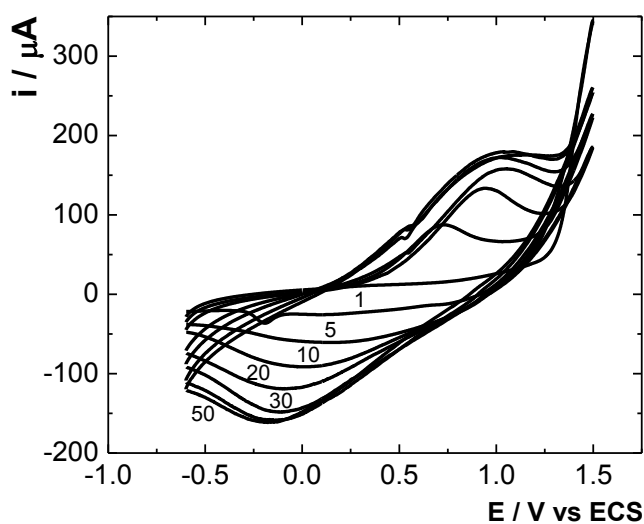


Figure 1. Voltammetric profile of $0.01 \text{ mol}\cdot\text{L}^{-1}$ py + $0.1 \text{ mol}\cdot\text{L}^{-1}$ LiClO₄ in CH₃CN, during the electropolymerization on a 0.07 cm^2 SS disc ($v = 50 \text{ mV}\cdot\text{s}^{-1}$), by successive potentiodynamic cycles (number of cycles on the respective curve).

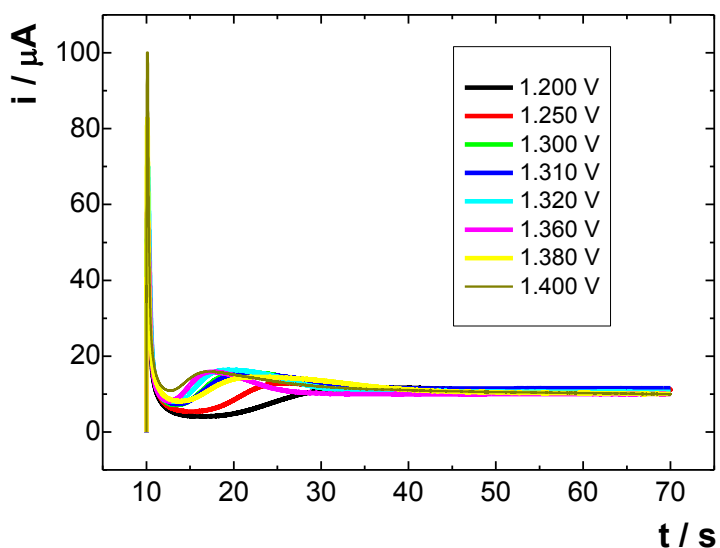
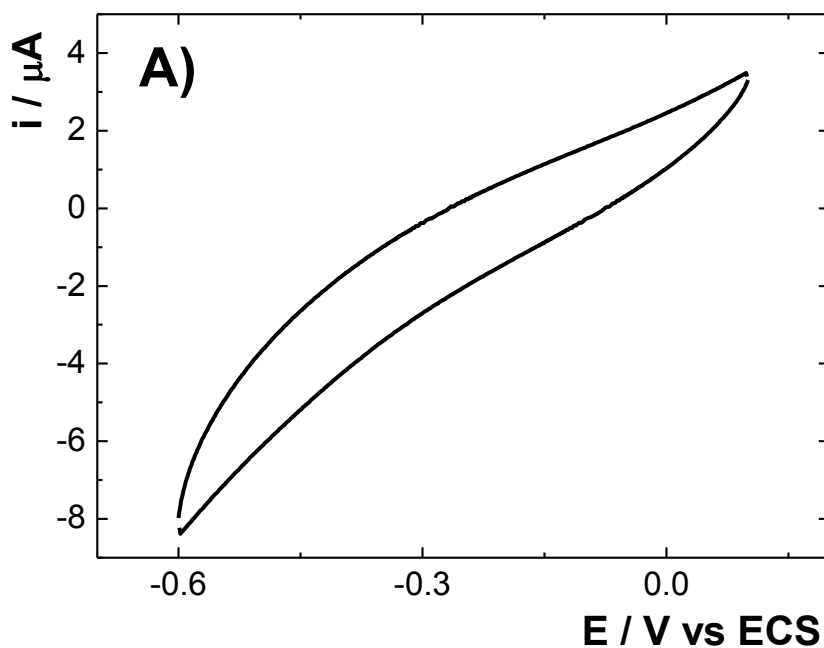


Figure 2. *i-t* transients recorded during py electro-polymerization by potentiostatic method (*E* showed in the insert). Interface: SS/0.01 py + 0.1 mol·L⁻¹ LiClO₄, CH₃CN.

In Fig. 2, the *i-t* transients evidences that, under the other experimental conditions used here, 1.36 V is the most suitable potential for py potentiostatic electro-polymerization.

Figures 3A and 3B depict the electrochemical responses in the *n-doping/undoping* and *p-doping/undoping* regions corresponding to Ppy electrochemical characterization in a supporting electrolyte solution.



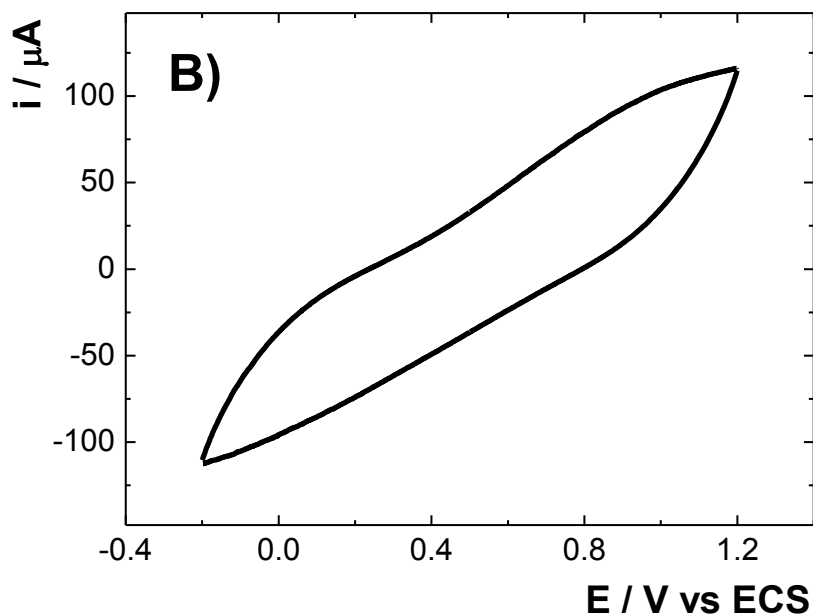


Figure 3. SS/Ppy electrode response: A) *n-doping/undoping* potential region; B) *p-doping/undoping* potential region.

Table 1 shows the respective negative (E_{cat}) and positive (E_{an}) limits within which this phenomenon takes place and the corresponding *n-doping/undoping* charges that revealed the process is fully reversible, since the cathodic/anodic charge quotients obtained for the electrochemical response (Fig. 3A) are very close to one.

Table 1. *n-doping* ($n-Q_d$) and *n-undoping* ($n-Q_u$) charge of electro-synthesized polymers on SS within the respective negative (E_{cat}) and positive (E_{an}) potential limits.

Polymer	E_{cat} (V)	E_{an} (V)	$n-Q_d$ (C)	$n-Q_u$ (C)	$n-Q_d: Q_u$
Ppy	-0.6	0.2	$8.6 \cdot 10^{-6}$	$8.5 \cdot 10^{-6}$	1.00

At the same time the respective charges calculated for *p-doping/undoping* indicated the process was fully reversible under the electro-synthesis conditions set forth herein, see Table 2.

Table 2. *p-doping* ($p-Q_d$) and *p-undoping* ($p-Q_u$) charge of polymers synthesized on SS electrodes within the respective limits of negative (E_{cat}) and positive (E_{an}) potential.

Polymer	E_{cat} (V)	E_{an} (V)	$p-Q_d$ (C)	$p-Q_u$ (C)	$p-Q_d: Q_u$
Ppy	-0.3	1.2	$5.20 \cdot 10^{-4}$	$5.21 \cdot 10^{-4}$	0.99

Optimum conditions, established by voltammetric characterization, were utilized to conduct the potentiostatic electro-polymerization. The same SS electrodes were employed in solutions similar to those already described as optimal, at a potential close to the anodic switching potential of each monomer. I-t transients shown as example in Fig. 4 indicated that when working under potentiostatic conditions in the NG region, a general behavior pattern exists that can be describe considering, firstly, that after the sudden initial current rise and subsequent exponential drop, ascribable to monomer oxidation, the current increases once more as nucleation, that gives rise to deposit growth (induction time τ), takes place as a function of such growth [27, 28].

Thus, as seen in other cases [29-36], it was observed that at potentials lower than the optimal one, the induction time, τ , is very high, while at higher potentials is very low and erratic with a total lack of reproducibility and, consequently, the generated film would be undergoing over-oxidation. On this basis, the most suitable potential for each of the studied monomers, when potentiostatic deposition was the technique of choice, are shown in Table 3.

Figure 4 shows time-current transients deconvolution, recorded during the potentiostatic preparation under the selected optimum conditions, in order to determine the respective NGM, as described in similar studies [20, 22, 28-36].

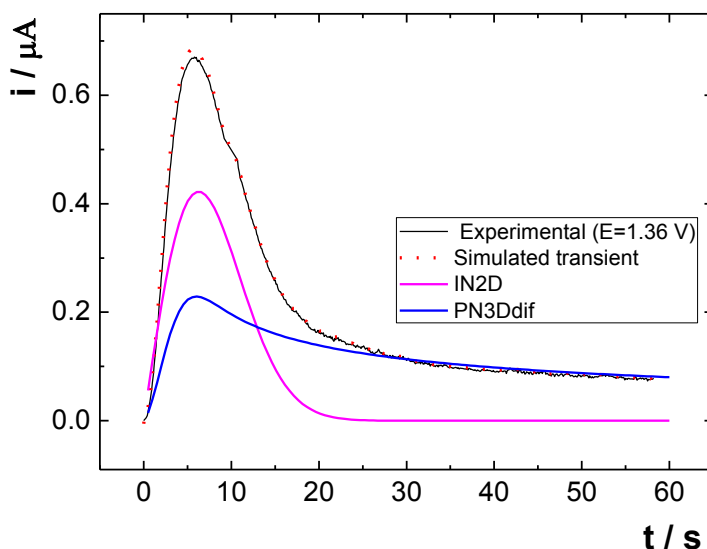


Figure 4. i-t transients deconvolution recorded for py at SS under the optimal working conditions.

The equations describing the contributions that enabled deconvoluting the obtained transients, corresponding to the respective NGM, were instantaneous nucleation with two-dimensional growth (IN2D) and progressive nucleation with diffusion-controlled three-dimensional growth (PN3D_{dif}) [31]:

$$i = P_1 \left[1 - e^{-P_2 t^2} \right] \quad (1)$$

$$i = t^{-1/2} P_3 \left[1 - e^{-P_4 t^2} \right] \quad (2)$$

The first contribution corresponds to equal-size nuclei (instantaneous nucleation) with a cylinder-shaped growth (two-dimensionally, parallel to the electrode), while the second consists of nuclei that appear and grow as a function of electrolysis time, parallel and normal to the electrode, hemisphere-shaped. Consequently, morphology consistent with this NGM prediction would be expected for these deposits. Nevertheless, it is worth noting that this mechanism is different from previous reports related to pyrrole derivatives on steel under the same conditions [15]. This fact would be, as expected, an evidence of monomer structure effect.

Parameters of equations (1) and (2) are displayed in Table 3, where M is the monomer molar mass, k is the growth parallel to the electrode rate constant, n is the number of electrons involved, F is the Faraday constant, h is the height of the monolayer, N_0 is the number of active surface sites, t is the time, ρ is the film density, C is the monomer bulk concentration, D is the diffusion coefficient, A_{dif} and N_{dif} are the nucleation rate constant in the steady state and the number of nuclei formed under diffusion control, respectively [25-36]. $P_1, P_2, P_3,$ and P_4 values obtained by transient deconvolution (Fig. 4) that allowed accurate simulation of the experimental transients, are summarized in Table 4.

Table 3. Expressions for the parameters of equations (1) and (2).

Parameter	Expression
P_1	$\frac{2\pi M k^2 n F h N_0 t}{\rho}$
P_2	$\frac{\pi N_0 M^2 k^2 t^2}{\rho^2}$
P_3	$\frac{n F C \sqrt{D}}{\sqrt{\pi}}$
P_4	$\frac{2\pi D A_{dif} N_{dif}}{3} \left(\frac{8\pi C M}{\rho}\right)^{1/2}$

Table 4. Numerical values of the parameters of equations (1) and (2) (Table 3) appropriate to deconvolute i/t transients recorded on SS (Fig.4).

Polymer	E (V)	P_1 (A·cm)	P_2 (ms ⁻²)	P_3 (mA·cm ⁻² ·s ^{1/2})	P_4 (ms ⁻²)	r^2
Ppy	1.36	1.10	0.18	0.07	0.15	0.9915

Values in Table 4 highlight, first, that r close to unity indicates a clear correlation between experimental and simulated transients and, consequently, the obtained NGM would be reliable. Besides, Fig. 4 shows that the profiles obtained by deconvolution or the sum of the curves calculated from the respective deconvolution equations (using the constants of Table 4) coincide almost exactly with the experimentally recorded transient.

Subsequently, to determine deposit morphology and particularly to validate the simulations leading to NGM determination, SEM was utilized to characterize the coating, Fig. 5A.

The micrograph in Fig. 5A allows ensuring that the morphology obtained for the deposit corroborates what was predicted from NGM, since semispheres with irregular size can be observed, consistent with a progressive nucleation mechanism.

To verify the morphological prediction from the NGM, the AFM technique was employed. The result that corroborates the prediction is depicted in Fig. 5B: two contributions are observed for Ppy, consistent with the NGM that presents two kinds of nuclei, with growth at different rates, causing a quite uneven surface.

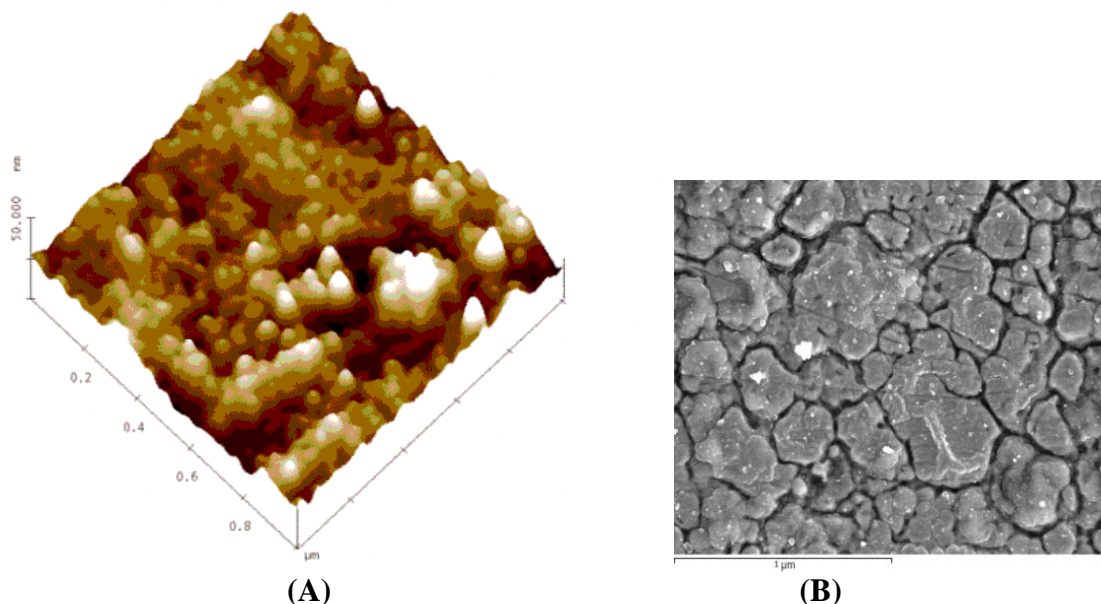


Figure 5. Images: A) SEM of Ppy on SS. B) AFM of Ppy on SS.

To round out the characterization and verify the NGM prediction, measurements were conducted by ATR and RAMAN spectroscopy. Figure 6 shows the ATR spectrum, where the bands are clearly assigned as follows: 3538 cm^{-1} ; C-NH *stretching* vibration corresponding to the pyrrole ring; 1630 cm^{-1} assigned to ring-deformation vibrations of pyrrole NH; 1207 cm^{-1} refers to C-N stretching vibrations of the py ring; 1443 cm^{-1} C=C, are assigned to stretching vibration of the py ring, and 1040 and 925 cm^{-1} corresponding to =C-H of the ring plane.

Thus, the assignment of these bands confirmed *in situ* interaction between electrode substrate (SS in this case) and polymer matrix, Ppy, [37-39].

Finally, measurements were conducted using Raman spectroscopy that corroborated the polymer obtention, Fig. 8, since it is possible to identify the following bands: 1545 cm^{-1} , corresponding to the $C_{\alpha}=C_{\beta}$ asymmetric stretching; 1423 cm^{-1} assigned to the $C_{\alpha}=C_{\beta}$ symmetric stretching; 1370 cm^{-1} the $C_{\beta}=C_{\beta}$ ring *stretching*; 1247 cm^{-1} ascribed to $C_{\alpha}=C_{\alpha'}$ *stretching* (inter-ring); 1224 cm^{-1} assigned to the $C_{\alpha}-N$ *stretching*, and 1110 cm^{-1} assigned to C-H [39-41].

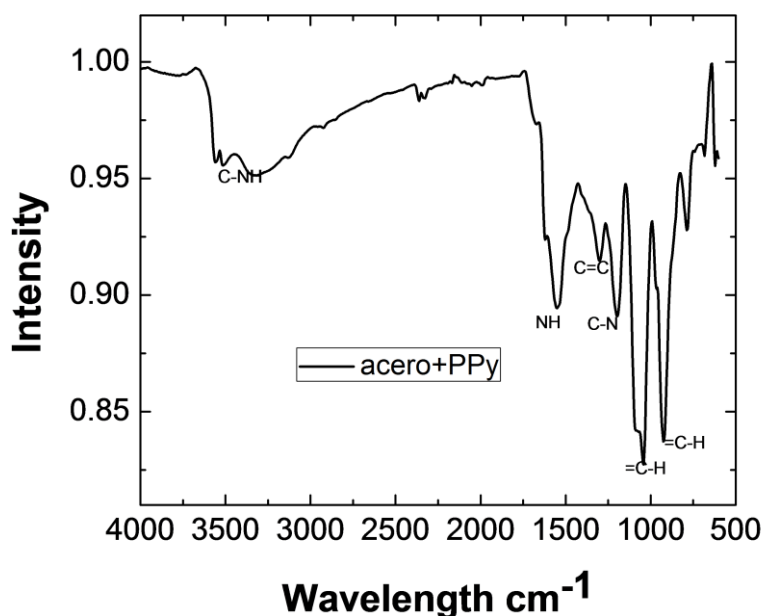


Figure 6. Ppy ATR spectrum.

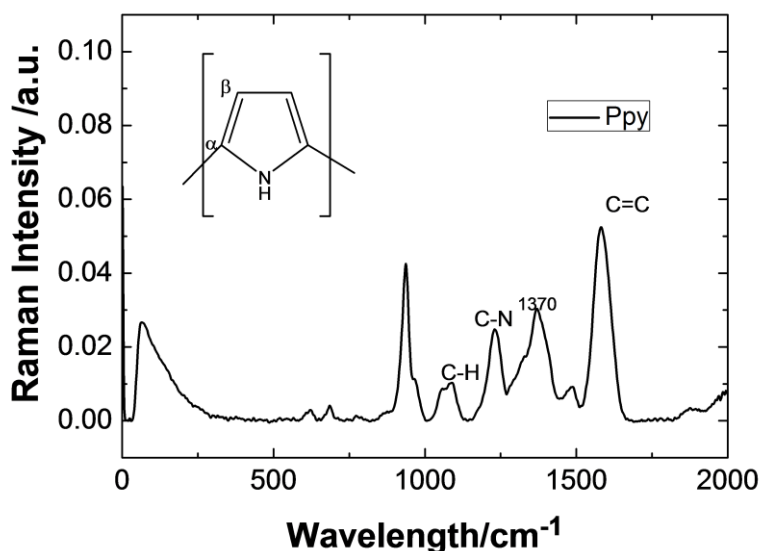


Figure 7. Ppy Raman spectrum.

NGM deconvolution of Ppy on steel, exhibited many differences with respect to pyrrole derivatives previously reported (3,4-ethylenedioxyppyrole (PEDOP) and 3,4 propylenedioxyppyrole (PRODOP)) [15], wherein the following contributions predominate: instantaneous nucleation with three-dimensional growth under charge-transfer control (IN3D_{ct}), however, a second contribution also exists, corresponding to a three-dimensional progressive nucleation under diffusion-controlled growth (PN3D_{dif}), the latter contribution also occurs for Ppy under the same electro-synthesis conditions,

indicating that the first contribution is governed by epoxy-alkyl chains for pyrrole derivatives. So, these results clearly demonstrated that the substituent chains govern the IN3D_{ct} contribution.

Ppy ATR and RAMAN characterization revealed, from signals assignment, that its conformational structure is flat. In addition as, unlike its derivatives (PEDOP and PPRODOP), Ppy lacks of substituents allowed its structure to be worked out this way.

4. CONCLUSIONS

Ppy was obtained on steel under the found optimum working conditions, exhibiting both n- and p-doping/undoping processes. Although the second charging process always presented greater charge than the first, both are practically reversible with regard to the respective charges involved.

Besides of characterization of p- and n-doping/undoping processes, that allow proposing and choosing the most appropriate starting unit, depending on the use in mind for the polymeric deposit, Ppy experimental transients were simulated. Two contributions to the overall process were found, one involving an instantaneous nucleation with two-dimensional growth (IN2D) and a second corresponding to a three-dimensional progressive nucleation with diffusion-controlled growth (PN3D_{dif}). The value of r very close to 1 for all simulations must be highlighted. Furthermore, the morphology associated with these NGMs correlates exactly with those experimentally determined by SEM and AFM. This allows shorter path for the choice of the starting unit and the experimental design to prepare the modified electrode according to their potential use.

ACKNOWLEDGMENTS

The authors thank CONICYT financial support through grants FONDECYT 1100055, and Ecos-Conicyt C09E02. GC Arteaga thanks CONICYT Scholarship 2009, Folio 57090049.

References

1. M. U. Sreekuttan, M. D. Vishal, K. P. Vijayamohanan, and K. Sreekumar, *J. Phys. Chem. C*, 114 (2010) 14654.
2. E. Smela, *Adv. Mater.*, 15 (2003) 481.
3. Z. Liu, J. Wang, V. Kushvaha, S. Poyraz, H. Tippur, S. Park, M. Kim, Y. Liu, J. Bar, H. Chene and X. Zhang, *Chem. Commun.*, 47 (2011) 9912.
4. J. Xia, L. Chena, and S. Yanagida, *J. Mater. Chem.*, 21 (2011) 4644.
5. L. Wang, X. Li, and Y. Yang, *React. Funct. Polym.*, 47 (2001) 125.
6. J. C. Vidal, E. García, and J. R. Castillo, *Anal. Chim. Acta.*, 385 (1999) 213.
7. T. E. Campbell, A. J. Hodgson, and G. G. Wallace, *Electroanal.*, 11 (1999) 215.
8. E. Smela, *J. Micromech. Microeng.*, 9 (1999) 1.
9. T. A. Skotheim, R. Elsenbaumer, and J. Reynolds, *Handbook of Conducting Polymers*, Marcel Dekker, New York (1998).
10. T. A. Skotheim, *Handbook of Conducting Polymers*, Vols. I and II, Marcel Dekker, New York (1986).
11. M. A. del Valle, G. Soto, L. Guerra, J. Vélez, and F. R. Díaz, *Polym. Bull.*, 51 (2004) 301.
12. M. Antilén, and F. Armijo, *J. Appl. Polym. Sci.*, 113 (2009) 3619.

13. M. Antilén, M. González, M. Pérez, M. A. Gacitúa, M. A. del Valle, F. Armijo, R. del Río, and G. Ramírez, *Int. J. Electrochem. Soc.*, 6 (2011) 901.
14. M. Antilén, D. Guzmán, M. A. del Valle, R. del Río, M. V. Letelier, G. Lagos, M. Escudey, C. Pizarro, *Int. J. Electrochem. Soc.*, 7 (2012) 5939.
15. G. C. Arteaga, M. A. del Valle, M. Antilén, F. R. Díaz, M. A. Gacitúa, P. P. Zamora, J. C. Bernède, L. Cattin, and G. Louarn, *Int. J. Electrochem. Sci.*, 7 (2012) 7840.
16. M. A. del Valle, G. Soto, L. Guerra, J. Vélez, and F. R. Díaz, *Polym. Bull.*, 51 (2004) 301.
17. R. Schrebler, M. A. del Valle, H. Gómez, C. Veas, R. Córdova, *J. Electroanal. Chem.*, 219 (1995) 380.
18. F. R. Díaz, M. A. del Valle, F. Brovelli, L. H. Tagle, and J. C. Bernède, *J. Appl. Polym. Sci.*, 89 (2003) 1614.
19. M. A. del Valle, P. Cury, and R. Schrebler, *Electrochim. Acta*, 48 (2002) 397.
20. L. Ugalde, J. C. Bernède, M. A. del Valle, F. R. Díaz, and P. Leray, *J. Appl. Polym. Sci.*, 84 (2002) 1799.
21. M. A. del Valle, L. Ugalde, F. R. Díaz, M. E. Bodini, and J. C. Bernède, *J. Appl. Polym. Sci.*, 92 (2004) 1346.
22. M. B. Camarada, P. Jaque, F. R. Díaz, and M. A. del Valle, *J. Polym. Sci. Pol. Phys.*, 49 (2011) 1723.
23. M. Romero, M. A. del Valle, R. del Río, and F. Armijo, *Int. J. Electrochem. Soc.*, 7 (2012) 10132.
24. M. B. Camarada, J. A. Olmos-Asar, M. M. Mariscal, and M. A. del Valle, *Mol. Simul.*, 38 (2012) 882.
25. M. A. del Valle, M. A. Gacitúa, E. D. Borrego, P. P. Zamora, F. R. Díaz, M. B. Camarada, M. Antilén, and J. P. Soto, *Int. J. Electrochem. Soc.*, 7 (2012) 2552.
26. G. East, and M. A. del Valle, *J. Chem. Ed.*, 77 (2000) 97.
27. M. A. del Valle, R. A. Santander, F. R. Díaz, M. Faúndez, M. Gacitúa, M. Antilén, and L. A. Hernández, *Int. J. Electrochem. Soc.*, 6 (2011) 6105.
28. M. A. del Valle, M. B. Camarada, F. R. Díaz, and G. East, *e-Polymers*, 72 (2008) 1.
29. M. A. del Valle, M. Gacitúa, L. I. Canales, and F. R. Díaz, *J. Chil. Chem. Soc.*, 54 (2009) 260.
30. R. Córdova, M. A. del Valle, A. Arratia, H. Gómez, and R. Schrebler, *J. Electroanal. Chem.*, 377 (1994) 75.
31. E. Horwood, *Instrumental Methods in Electrochemistry*; Southampton Electrochemistry Group, 1985.
32. R. Turcu, M. Brie, G. Leising, V. Tosa, A. Mihut, A. Niko, and A. Bot, *Appl. Phys. A.*, 67 (1998) 283.
33. H. Kate, O. Nisbikawa, T. Mats, S. Honma, and H. Kokados, *J. Phys. Chem.*, 95 (1991) 6014.
34. X. Wang, H. Tang, X. Li, and X. Hua, *Int. J. Mol. Sci.*, 10 (2009) 5257.
35. H. Nguyen, M. C. Bernard, B. Garcia-Renaud, and C. Deslouis, *Synthetic. Met.*, 140 (2004) 287.
36. F. Chen, J. Zhang, F. Wang, and G. Shi, *J. Appl. Polym. Sci.*, 89 (2003) 3391.